Solution Structure of a Naturally-Occurring Zinc−Peptide Complex Demonstrates that the N-Terminal Zinc-Binding Module of the Lasp-1 LIM Domain Is an Independent Folding Unit[†,‡]

Anna Hammarström,[§] Kurt D. Berndt,[§] Rannar Sillard,[§] Knut Adermann,[||] and Gottfried Otting*[,§]

Department of Medical Biochemistry and Biophysics, Karolinska Institute, S-171 77 Stockholm, Sweden, and Lower Saxony Institute of Peptide Research, Feodor-Lynen-Strasse 31, D-30625 Hannover, Germany

Received May 15, 1996; Revised Manuscript Received July 29, 1996[⊗]

ABSTRACT: The three-dimensional solution structure of the 1:1 complex between the synthetic peptide ZF-1 and zinc was determined by ^{1}H NMR spectroscopy. The peptide, initially isolated from pig intestines, is identical in sequence to the 30 N-terminal amino acid residues of the human protein Lasp-1 belonging to the LIM domain protein family. The final set of 20 energy-refined NMR conformers has an average rmsd relative to the mean structure of 0.55 Å for the backbone atoms of residues 3−30. Calculations without zinc atom constraints unambiguously identified Cys 5, Cys 8, His 26, and Cys 29 as the zinc-coordinating residues. LIM domains consist of two sequential zinc-binding modules and the NMR structure of the ZF-1−zinc complex is the first example of a structure of an isolated module. Comparison with the known structures of the N-terminal zinc-binding modules of both the second LIM domain of chicken CRP and rat CRIP with which ZF-1 shares 50% and 43% sequence identity, respectively, supports the notion that the zinc-binding modules of the LIM domain have a conserved structural motif and identifies local regions of structural diversity. The similarities include conserved zinc-coordinating residues, a rubredoxin knuckle involving Cys 5 and Cys 8, and the coordination of the zinc ion by histidine N^{δ} in contrast to the more usual coordination by N^{ϵ} observed for other zinc-finger domains. The present structure determination of the ZF-1−zinc complex establishes the N-terminal half of a LIM domain as an independent folding unit. The structural similarities of N- and C-terminal zinc-binding modules of the LIM domains, despite limited sequence identity, lead to the proposal of a single zinc-binding motif in LIM domains. The coordinates are available from the Brookhaven protein data bank, entry 1ZFO.

Since their first description in TFIIIA (Klug & Rhodes, 1987), zinc-finger domains have been found to constitute the DNA-binding motifs in many proteins (Kaptein, 1993). The zinc ion in a zinc-finger domain is tetrahedrally coordinated by either cysteine thiolates or histidine imidazoles (Schwabe & Klug, 1994). Depending on the position of the coordinating cysteine and histidine residues in the amino acid sequence, CCHH, CCHC, CHCC, HCCC, and CCCC zinc-finger motifs have been described and characterized structurally (Schwabe & Klug, 1994). Here we report the three-dimensional solution structure of a naturally-occurring zinc−peptide complex with a CCHC zinc-binding motif determined by 2D ^{1}H NMR[1] spectroscopy. The peptide contains 30 amino acids and was named ZF-1 for its sequence homology with zinc-finger domains (Sillard et al., 1993). Subsequently, ZF-1 was recognized as being homologous to an N-terminal zinc-binding module of a LIM domain.

Proteins containing the zinc-binding LIM domain have diverse functions and are found in a wide variety of species (Sanchez-Garcia & Rabbitts, 1994; Taira et al., 1995). The name LIM comes from the three transcription factors in which it was first observed, namely, Lin-1, Isl-1, and Mec-3 (Freyd et al., 1990; Karlsson et al., 1990). The LIM domain is known to bind one zinc ion within each of two homologous but not identical zinc-binding modules (Michelsen et al., 1993; Kosa et al., 1994). The consensus LIM domain sequence is [C-$(X)_2$-C-$(X)_{16-23}$-(H,C,D)-$(X)_2$-(C,E,H)]-$(X)_2$-[C-$(X)_2$-C-$(X)_{16-21}$-C-$(X)_{2-3}$-(C,H,D)], where C, H, D, E, and X denote cysteine, histidine, aspartic acid, glutamic acid, and any of the common 20 amino acids, respectively. The LIM domains themselves are often repeated two to four times within the protein sequence and can be found in combination with homeodomains or kinases, but proteins containing LIM domains only have also been identified (Gill, 1995). The

[†] This work was supported by grants from the Swedish Natural Science Research Council (Project 10161) and the Wallenberg Foundation.

* Author to whom correspondence should be addressed.

[‡] PDB-ident code: 1ZFO (coordinates), R1ZFOMR (constraints).

[§] Karolinska Institute, MBB.

[||] Lower-Saxony Institute of Peptide Research.

[⊗] Abstract published in *Advance ACS Abstracts,* September 15, 1996.

[1] Abbreviations: COSY, two-dimensional correlated spectroscopy; CRP, cysteine-rich protein; CRIP, cysteine-rich intestinal protein; d_{NN}, $d_{\alpha N}$, $d_{\beta N}$, NOE observable distances between amide, α and β proton of residue i, and the amide proton of a residue with a higher sequence number, respectively; DIEA, *N*,*N*-diisopropylethylamine; HOBt, 1-hydroxybenzotriazole; TBTU, *O*-benzotriazolyl-*N*,*N*,*N*′,*N*′-tetramethyluronium tetrafluoroborate; DMF, *N*,*N*-dimethylformamide; Fmoc, 9-fluorenylmethyloxycarbonyl; MeCN, acetonitrile; NMR, nuclear magnetic resonance; NOE, nuclear Overhauser effect; NOESY, two-dimensional NOE spectroscopy in the laboratory frame; PEG−PS, polyethyleneglycol polystyrene; rmsd, root mean square deviation; ROE, nuclear Overhauser effect in the rotating frame; ROESY, two-dimensional NOE spectroscopy in the rotating frame; RP-HPLC, reverse-phase high-pressure liquid chromatography; SH3, src homology region 3; TOCSY, two-dimensional total correlation spectroscopy; TPPI, time-proportional phase incrementation; ZF-1, zinc-finger peptide 1.

S0006-2960(96)01149-X CCC: $12.00

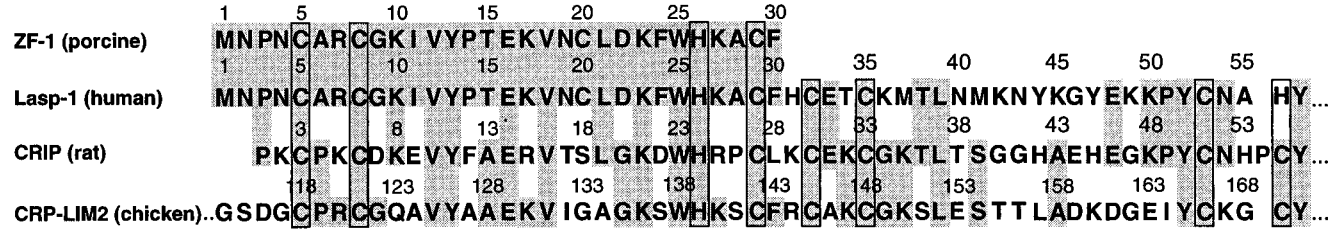

FIGURE 1: Amino acid sequence comparison of the ZF-1 peptide with the LIM domains of the protein Lasp-1 (Tomasetto et al., 1995a,b), CRIP (Pérez-Alvarado et al., 1996), and CRP (Pérez-Alvarado et al., 1994). Identical residues are shaded and the LIM consensus sequence is identified with boxes.

LIM domain-containing proteins include transcription factors (Freyd et al., 1990; Karisson et al., 1990; Way & Chalfie, 1988; Cohen et al., 1992; Mizuno et al., 1994) and cytoskeletal components (Crawford et al., 1992, 1994), and some seem to be involved in regulation of cell growth and cellular differentiation (Arber et al., 1994; Weiskirchen et al., 1995). The specific function of the LIM domain is at present not known, but it has recently been demonstrated that a LIM domain can act as an interface for protein−protein interactions (Schmeichel & Beckerle, 1994; Feuerstein et al., 1994). Another possible function of the LIM domain is illustrated by the cysteine-rich intestinal protein (CRIP), which consists of a single LIM domain and may play a role in intestinal zinc transport (Hempe & Cousins, 1991; O'Dell, 1992).

To date, the C-terminal LIM domain from the chicken cysteine-rich protein (CRP LIM2) (Pérez Alvarado et al., 1994) and the rat CRIP (Pérez-Alvarado et al., 1996) are the only reported 3D structures of LIM domains. The two independent zinc-binding modules are structurally homologous. They are also structurally related to the DNA-binding zinc-finger domains of nuclear hormone receptors (Luisi et al., 1991) and GATA-1 (Omichinski et al., 1993), suggesting that LIM domains may bind to DNA. The wide range of functions suggested for LIM domains may be expected to result in at least some structural diversity.

The ZF-1 peptide shares 100% sequence identity with the N-terminal 30 amino acids of the Lasp-1 protein (Figure 1). The gene of Lasp-1 (MLN 50) was recently identified and found to be overexpressed in breast cancer cell lines. Based on its amino acid sequence homology, the 261 amino acid Lasp-1 protein contains a LIM-domain at its amino terminus and an SH3 domain in the carboxy terminal part (Tomasetto et al., 1995a,b). MLN 50 was originally identified from a cDNA library of breast cancer metastasis, but was also found to be expressed at a basal level in normal tissue. It is thought that the protein may be involved in a signaling pathway contributing to cell transformation and/or tumor progression (Tomasetto et al., 1995a,b). ZF-1 was initially isolated from pig intestines (Sillard et al., 1993). Because of the close relationship between human and porcine proteins, it is likely that ZF-1 is derived from a porcine Lasp-1 protein. This is also supported by the fact that ZF-1, like most eukaryotic proteins, is acetylated at the amino terminus. Although *in vivo* cleavage of porcine Lasp-1 is a likely source of ZF-1, proteolysis during the isolation procedure or *in vivo* synthesis cannot be entirely excluded.

The sequence identity between the LIM domains of CRP and Lasp-1 is 50% between the first zinc-binding modules and 39% for the entire LIM domain, and the corresponding values for CRIP are 43% and 46% (Figure 1). While the biological function of ZF-1 is unclear, the present work shows that the ZF-1−zinc complex is a structurally independent folding unit with well-defined conformation. This is the third example of an N-terminal zinc-binding module of a LIM domain for which the three-dimensional solution structure has been determined and the first in the absence of a C-terminal module. The comparison between the structures of ZF-1, CRIP, and CRP LIM2 allows one to address the question of structural conservation and diversity between LIM domains from different proteins.

MATERIALS AND METHODS

NMR Sample Preparation. Peptide synthesis (Atherton & Sheppard, 1989) was carried out on a preloaded Fmoc-L-Phe-PEG-PS resin (loading 0.17 mmol/g, PerSeptive) using a PerSeptive 9050 automated peptide synthesizer. In general, couplings were performed with a 4-fold excess of Fmoc-amino acids in the presence of TBTU/DIEA/HOBt (1:1:0.5, v:v:v) for 30 min. Fmoc groups were cleaved with 20% piperidine in DMF for 10 min. Coupling of methionine was carried out at 0 °C with acetic anhydride/pyridine/DMF (10:1:89, v:v:v) for 10 min. Resin cleavage and deprotection were performed with trifluoroacetic acid/ethanedithiol/water (94:3:3, v:v:v) for 90 min. After precipitation of the crude peptide by addition of cold *tert*-butyl methyl ether, the peptide was purified by preparative RP-HPLC (Vydac C18, 300, 10 μm, 25 × 250 mm; flow rate, 10 mL/min; buffer A, 0.6% TFA in water; buffer B, 0.5% TFA in MeCN/water 4:1; detection at 230 nm). Fractions containing absorbance peaks were pooled, and the final product was checked with analytical RP-HPLC (Vydac C18) and capillary zone electrophoresis (BioFocus 3000, Bio-Rad). Electrospray mass spectrometry (Sciex API III, Perkin-Elmer), gas phase sequencing (473A Protein Sequencer, Applied Biosystems), and amino acid analysis (Aminoquant 1090L, Hewlett Packard) showed correct mass, amino acid sequence, and amino acid composition of the purified peptide.

The NMR sample was prepared by dissolving 3.5 mg of the lyophilized peptide in 0.5 mL of a degassed mixture of 90% H_2O/10% D_2O containing a 10% molar excess of $ZnSO_4$. Subsequently, the pH was increased from approximately 2.3 by adding deuterated sodium acetate under nitrogen atmosphere until the complex was formed. The progress of the titration was monitored by recording 1D ^1H NMR spectra. Attempts to form a Cd−peptide complex using $CdSO_4$ instead of $ZnSO_4$ were unsuccessful, leading to a precipitated sample. A sample dissolved in D_2O was prepared by lyophilizing the NMR sample and dissolving it in D_2O (99.95%).

NMR Spectra. All NMR data were collected at a ^1H frequency of 600 MHz on a Bruker DMX-600 NMR spectrometer. Data were analyzed using the programs PROSA (Güntert et al., 1992) and XEASY (Bartels et al., 1995). All spectra were recorded at 25 °C, except for data

recorded at 4 °C to identify slowly exchanging amide protons. The spectra recorded for the resonance assignment of the ZF-1−zinc complex included DQF-COSY (Rance et al., 1983; Bodenhausen et al., 1984), clean TOCSY using the clean CITY mixing scheme (Briand & Ernst, 1991) with a mixing time of 100 ms, and NOESY (Ernst et al., 1987) with a mixing time of 100 ms. For unambiguous assignments of degenerate methylene chemical shifts, a double-quantum experiment (Braunschweiler et al., 1983) was also recorded. In these spectra the water signal was suppressed by selective pre-irradiation of the water resonance. The upper distance limits were collected from a ROESY spectrum recorded with a spin-lock purge pulse for water suppression (Otting et al., 1991) and a mixing time of 100 ms. The spectrum was recorded using $t_{1max} = 60$ ms, $t_{2max} = 230$ ms, and 1024 × 4096 data points. The total experimental time was 63 h. Exchange cross-peaks observed in this spectrum between the water resonance and the amide protons identified those amide protons for which the exchange rates with water were faster than 10 s^{-1}. Coupling constants, $^3J_{H\alpha HN}$, were obtained from this experiment using a line fitting procedure of the in-phase cross-peaks involving amide protons (Szyperski et al., 1992). Qualitative information about the size of $^3J_{H\alpha H\beta}$ coupling constants was obtained from a series of clean TOCSY experiments recorded with mixing times of 4, 11, and 21 ms, and from a small flip angle COSY experiment (Aue et al., 1976) performed in D_2O solution. Slowly exchanging amide protons were identified from a NOESY experiment recorded at 4 °C during 1.5 h immediately after dissolving a freshly lyophilized sample in D_2O. Amide protons with exchange rates $<10^{-4}$ s^{-1} were observed in this spectrum.

Structure Calculation. The strategy for structure determination was similar to that used for the structure determination of PEC-60 (Liepinsh et al., 1994). The cross-peaks in the ROESY spectrum were assigned and integrated using the program XEASY. The program CALIBA (Güntert et al., 1991a) was used to translate the cross-peak volumes into upper distance limit constraints. The volumes of all cross-peaks except those between side chain protons (excluding β-protons) and involving methyl groups were converted into upper distance bounds, b, using a $1/b^6$ dependence. For the ROEs between side chain protons or involving methyl groups, a $1/b^4$ dependence was used to compensate for increased ROE intensities observed with flexible side chains (Güntert et al., 1991b). Stereospecific assignments for some of the β-methylene protons and constraints for the dihedral angles ϕ, ψ, and χ^1 were initially obtained using the program HABAS (Güntert et al., 1989) with intraresidual and sequential NOE distance constraints as well as $^3J_{H\alpha HN}$ and $^3J_{H\alpha H\beta}$ coupling constants as input.

The structure calculations were performed with the distance geometry program DIANA (Güntert et al., 1991a) using the REDAC strategy (Güntert & Wüthrich, 1991). The DIANA library was modified to include the acetylated N-terminus and the zinc ion. The zinc coordination site was identified by initial structure calculations performed without the zinc ion and without any assumptions on zinc coordination (see Results and Discussion). Subsequent structure calculations included zinc and artificial upper and lower distance limit constraints to enforce the tetrahedral coordination found in other zinc-binding proteins (Frankel et al., 1987; Párraga et al., 1988), including a LIM domain protein (Michelsen et al., 1993). Zinc was introduced as an atom covalently attached to the sulfur of Cys 5 with a bond length of 2.30 Å and a Zn−S^γ−C^β bond angle of 96°. The geometry with respect to the other coordinating residues, Cys 8, His 26, and Cys 29, was restrained by upper and lower distance limits yielding the following allowed bond length intervals (in Å): 2.25 ≤ Cys S^γ-Zn ≤ 2.35 and 1.95 ≤ His $N^{\delta 1}$−Zn ≤ 2.05. Upper and lower distance limits were also used for the His C^γ, His $C^{\epsilon 1}$, and Cys C^β distances to the zinc and the Cys S^γ−Cys S^γ distances allowing a 0.2 Å distance interval consistent with a tetrahedral coordination of the zinc ion and sp^2 hybridization of the His $N^{\delta 1}$ atom. The limits used were (in Å) 2.99 ≤ Cys C^β−Zn ≤ 3.19, 3.73 ≤ Cys S^γ−S^γ ≤ 3.93, 2.93 ≤ His C^γ−Zn ≤ 3.13, and 2.88 ≤ His $C^{\epsilon 1}$−Zn ≤ 3.08. The distance bounds and bond angles were derived from the corresponding values observed for the protonated cysteine and histidine residues in the DIANA library by lengthening the S^γ−H and $N^{\delta 1}$−H bonds and replacing the proton by a Zn atom.

In the last round of the DIANA calculations, lower distance limits of 3 Å were introduced for those interproton distances that were shorter than 3 Å in the previously calculated structures but for which no corresponding cross-peak was observed in the ROESY and NOESY spectra. A total of 153 lower limits were thus identified.

Energy Refinement. Of 100 conformers calculated, the 30 conformers with the lowest target function were subjected to restrained energy minimization using the AMBER94 force field and parameters (Cornell et al., 1995) as implemented in the program OPAL (P. Luginbühl, P. Güntert, M. Billeter, and K. Wüthrich, unpublished results), including pseudoenergy terms for the dihedral angle constraints and upper distance limit constraints. Lower distance limit constraints were not used for the energy minimization. A total of 2500 steps of conjugate gradient minimization were carried out in the presence of a 6 Å shell of H_2O using a constant dielectric constant for electrostatic interactions.

The AMBER94 library (Cornell et al., 1995) was also modified to accommodate the N-terminal acetyl group and the zinc ion. A formal charge of +2 and a radius of 1.10 Å were attributed to the zinc ion which was covalently linked to the S^γ of Cys 5 with a bond length of 2.30 Å. The same value was introduced for the bonds Cys 8 S^γ−Zn and Cys 29 S^γ−Zn. The bond His 26 $N^{\delta 1}$−Zn was set to 2.05 Å. Bond angles were introduced for the following sets of atoms to ensure tetrahedral coordination of the zinc ion and the coordinating sulfur atoms and sp^2 hybridization of the coordinating His $N^{\delta 1}$ atom: S^γ−Zn−S^γ and S^γ−Zn−$N^{\delta 1}$ angles were set to 109.5°, C^β−S^γ−Zn was set to 96°, and C^γ−$N^{\delta 1}$−Zn and $C^{\epsilon 1}$−$N^{\delta 1}$−Zn were set to 126°.

The restrained-energy minimization used the angle constraints derived by HABAS for all angles except ψ. In addition, the constraints from the last level of DIANA calculations were used for the χ^1 angle constraints of the residues with stereospecifically assigned β-protons. Of the 30 energy-refined conformers, the 20 conformers with the lowest AMBER energy were selected to represent the solution structure of the ZF-1−zinc complex. These conformers were analyzed with the program XAM (Xia, 1992) which includes the algorithm of Richmond (1984) for the calculation of solvent accessibility. The program XAM was modified to detect hydrogen bonds with sulfur atoms. Finally, the programs MOLMOL (Koradi et al., 1996) and RIBBONS (Carson, 1991) were used to analyze the conformers and generate graphics for the visualization.

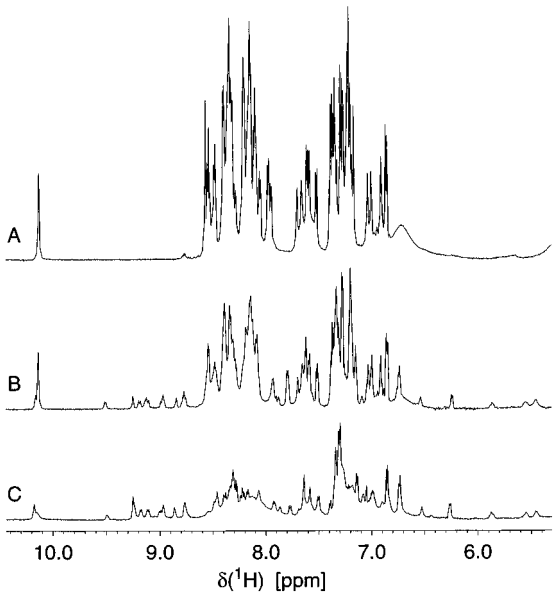

FIGURE 2: ^{1}H NMR spectra of a solution containing 2.0 mM ZF-1 and 2.2 mM $ZnSO_4$ in 90% H_2O/10% ^2H_2O at 25 °C and variable concentrations of deuterated sodium acetate. The spectral region containing the amide and aromatic proton resonances is shown. (A) Without sodium acetate, pH = 2.3; (B) with 10 mM sodium acetate, pH ≈ 4; (C) with 60 mM sodium acetate, pH = 5.5

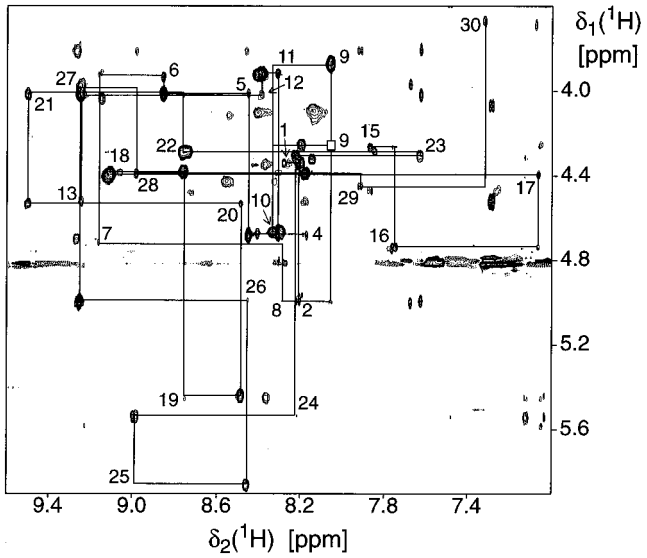

FIGURE 3: Spectral region of a ROESY spectrum of the ZF-1−zinc complex recorded with the sample of Figure 2C. The spectral region containing the $H^{\alpha}-H^{N}$ cross-peaks is shown. Negative and positive levels are plotted with solid and broken lines, respectively. The sequential assignment pathway is indicated for the entire peptide by straight lines, with numbers indicating the positions of the intraresidual $H^{\alpha}-H^{N}$ cross-peaks. A box identifies the expected position of one of the intraresidual $H^{\alpha}-H^{N}$ connectivities of Gly 9, which was too weak to be observed in this spectrum.

RESULTS AND DISCUSSION

Zinc−Peptide Complex Formation. The ZF-1−zinc complex was formed by titrating a 2.0 mM solution of ZF-1 containing a 10% excess of $ZnSO_4$ at approximately pH 2.3 with deuterated sodium acetate. Complex formation was monitored by 1D ^{1}H NMR spectra (Figure 2). The spectrum at low pH (Figure 2A) was identical to that in the absence of zinc (data not shown), corresponding to uncomplexed ZF-1 peptide. The chemical shift dispersion at this pH was characteristic of a random coil conformation. With increasing pH, a new set of peaks appeared with a chemical shift dispersion more characteristic of a structured polypeptide (Figure 2B and 2C). The ZF-1−zinc complex began to form at about pH 3.5. The chemical exchange between free and zinc-complexed ZF-1 was sufficiently slow to enable the observation of separate resonances for the complexed and uncomplexed species. At about pH 4.5, approximately one-third of the peptide had formed the complex as indicated by the integrals in the 1D spectra (Figure 2B). Raising the pH further by adding more sodium acetate did not lead to the formation of more ZF-1−zinc complex. Instead, the signals of the residual two-thirds of the ZF-1 peptide broadened (e.g., the indol NH signal of Trp 25 at about 10.1 ppm, Figure 2B and 2C), but their chemical shifts did not change from the random coil values observed at low pH. These results were reproduced in repeated titration experiments at different sample concentrations.

There are at least two plausible explanations for this behavior. The first is that the peptide is chemically heterogeneous such that only one-third of the preparation is capable of forming a well-defined high-affinity complex with zinc. The line-broadening observed in NMR spectra is consistent with aggregation of the remaining two-thirds of the sample since it affected all ^{1}H resonances uniformly and raising the pH above 5.5 resulted in precipitation. NOE and ROE experiments showed no evidence for chemical exchange between the relatively narrow lines of the well-defined complex and the broad signals from the remainder of the sample. The presence of heterogeneity was also suggested by capillary electrophoresis of the freshly synthesized and purified peptide which showed two poorly resolved peaks of equal intensities. Electrospray mass spectroscopy of an aliquot taken from the NMR sample of Figure 2C showed the expected molecular mass of the ZF-1−zinc complex and only very small amounts of oxidized peptide with intra- and intermolecular disulfide bridges. Limited racemization of some L-amino acids (particularly His) during peptide synthesis is a well-known problem in solid phase peptide synthesis (Gross & Meienhofer, 1981) and would support this interpretation. A second explanation is that a majority of the peptide is trapped in a misfolded, structurally ill-defined state resulting in only one-third properly folded complex. Similar difficulties in forming a zinc−peptide complex from a chemically synthesized peptide have also been encountered for *Desulfovibrio gigas* desulforedoxin (B. J. Goodfellow and J. J. G. Moura, personal communication), which were absent when the recombinant peptide was used.

Resonance Assignments. The present structure determination was performed for the well-defined high-affinity ZF-1−zinc complex at 25 °C and a pH of about 5.5 at a concentration of the ZF-1−zinc complex of 0.6 mM. The sequential resonance assignments were obtained from the ^{1}H homonuclear experiments in the conventional way (Wüthrich, 1986). The ^{1}H chemical shifts for the ZF-1−zinc complex are available as supporting information. The sequential assignment pathway *via* $d_{\alpha N}(i,i+1)$ connectivities is shown in the ROESY spectrum of Figure 3. The spectrum demonstrates that the broadened signals present in the 1D spectrum between 8.0 and 8.5 ppm did not affect the spectral quality, since they relaxed rapidly during the spin-lock mixing. Figure 4 shows an overview of selected sequential and medium-range connectivities. Both prolines were found to be in the *trans* configuration, as evidenced by the presence

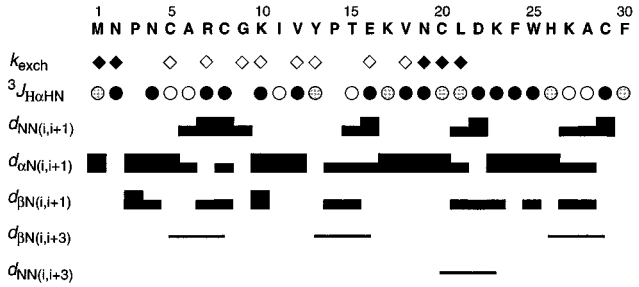

FIGURE 4: Overview of the amide proton exchange rates, k_{exch}, $^3J_{H\alpha HN}$ coupling constants, and ROE connectivities observed in the ROESY spectrum of Figure 3. Open diamonds identify residues for which amide proton exchange rates $k_{exch} < 10^{-4}$ s^{-1} were measured at 4 °C. Filled diamonds indicate $k_{exch} > 10$ s^{-1} at 25 °C. White, gray, and black circles indicate $^3J_{H\alpha HN} < 5.0$ Hz, $5.0 < {}^3J_{H\alpha NH} < 8.0$ Hz, and $^3J_{H\alpha HN} > 8.0$ Hz, respectively. Sequential ^{1}H−^{1}H ROE connectivities with residue *i* are displayed as black rectangles the heights of which reflect the cross peak intensities; connectivities between residues *i* and *i*+3 are displayed as lines connecting the two residues involved.

of sequential $H^{\alpha}-H^{\delta}$ ROEs. Cross-peaks were observed between the imidazole $H^{\epsilon 2}$ resonance at 11.89 ppm and the $H^{\delta 2}$ proton of His 26 in COSY and TOCSY spectra. In addition, the imidazole $H^{\epsilon 2}$ resonance showed ROEs to both the $H^{\delta 2}$ and the $H^{\epsilon 1}$ protons. This showed that $N^{\epsilon 2}$ and not $N^{\delta 1}$ was protonated, leaving $N^{\delta 1}$ to bind to the zinc ion. Five of the 16 non-degenerate pairs of β methylene protons were stereospecifically assigned by the program HABAS, and five additional pairs were identified by the program GLOMSA (Güntert et al., 1991a). In addition, the α-protons of Gly 9, the methyl groups of Val 12, and the side chain amide protons of Asn 2 were stereospecifically assigned by GLOMSA. The side chain amide protons of the other asparagine residues were stereospecifically assigned by comparing the relative intensities of the $H^{\beta 2/\beta 3}-N^{\delta}H_2$ ROESY cross-peaks.

Dihedral Angle Constraints. The smal flip angle COSY and short mixing time TOCSY spectra were evaluated to obtain measurements for $^3J_{H\alpha H\beta}$. For the residues 8 and 20, both $H^{\alpha}-H^{\beta 2/\beta 3}$ cross-peaks were missing from the small flip angle COSY and the short mixing time TOCSY spectra either because both $^3J_{H\alpha H\beta}$ were small, or because of saturation of the H^{α} resonance by the water saturation. The $H^{\beta 2/\beta 3}$ proton pairs had degenerate chemical shifts for residues 22, 24, 26, 29 and probably 17. Conformational averaging over more than one χ^1 rotamer was indicated for Met 1, Asn 19, and Lys 27 by $^3J_{H\alpha H\beta}$ coupling constants ranging between 5.0 and 8.0 Hz and similar $H^{\alpha}-H^{\beta 2/\beta 3}$ as well as similar $H^{N}-H^{\beta 2/\beta 3}$ ROE intensities. For the remaining pairs of β-methylene protons, the observation of one small and one large $^3J_{H\alpha H\beta}$ value was associated with values of 3.5 ± 2 and 11.5 ± 2 Hz, respectively, corresponding to χ^1 population ranges which include fully staggered rotamers. The $^3J_{H\alpha HN}$ coupling constants were used with error ranges of ±1 Hz. To avoid generating constraints for conformationally averaged residues, the $^3J_{H\alpha HN}$ coupling constants were considered only if they were either less than 5.0 Hz or greater than 8.0 Hz. A total of 20 $^3J_{H\alpha HN}$ coupling constants and eight pairs of $^3J_{H\alpha H\beta}$ coupling constants were used as input to the program HABAS.

Determination of the Three-Dimensional Structure. Initial structures were calculated without the zinc ion using only upper distance limit constraints derived from ROEs and dihedral angle constraints derived from the program HABAS.

Table 1: Quality Assessment of the NMR Structure[a] of the ZF-1−Zinc Complex

	value ± standard deviation
target function[b]	0.62 ± 0.24 Å^2
maximum violations of	
upper distance constraints[c]	0.10 ± 0.01 Å
torsion angle constraints[c]	1.85° ± 0.21°
lower distance constraints[b]	0.15 ± 0.07 Å
average violations per constraint for	
upper distance[c]	0.009 ± 0.001 Å
torsion angles[c]	0.33° ± 0.07°
lower distances[b]	0.003 ± 0.001 Å
average pairwise rmsd before and after energy minimization	
backbone[d]	0.59 ± 0.07 Å
heavy atoms[e]	0.91 ± 0.06 Å
average rmsd with respect to the mean structure	
backbone[f]	0.55 ± 0.11 Å
heavy atoms[g]	1.12 ± 0.14 Å

[a] The NMR structure is represented by the group of 20 refined DIANA conformers. [b] After DIANA calculations. [c] After restrained energy minimization. [d] For the atoms N, C^{α}, and C′ of residues 3−30 of corresponding structures before and after energy minimization. [e] For all heavy atoms of residues 3−30 of corresponding structures before and after energy minimization. [f] With respect to the mean structure after superposition for minimum rmsd of the atoms N, C^{α}, and C′ of residues 3−30. [g] With respect to the mean structure after superposition for minimum rmsd of all heavy atoms, excluding the zinc atom, of residues 3−30.

The side chains of Cys 5, Cys 8, His 26, and Cys 29 were oriented toward each other in these structures, identifying these residues as the zinc-coordinating residues. On the basis of amino acid sequence comparison, these residues also constitute the zinc coordination site in the LIM domain sequences (Kosa et al., 1994). Cys 20 was found in all structures to be remote to the zinc-binding site (Figure 6B).

The input for the final structure calculations consisted of 187 upper distance limit constraints, 153 lower distance limit constraints and 64 dihedral angle constraints. This input included ten upper and ten lower distance constraints to restrict the zinc coordination site (see Materials and Methods). Of the 177 non-redundant NOE constraints, 73 were intraresidual, 49 sequential, 22 medium range, and 33 involved protons in residues separated by more than five amino acids in ZF-1. The Trp 25 side chain was found to be in more than one conformation as reflected by two sets of NOE constraints that could not be fulfilled simultaneously. Four NOE constraints, Cys 20 H^{N}−Trp 25 $H^{\zeta 3}$ (4.5 Å), Phe 24 H^{α}−Trp 25 $H^{\epsilon 3}$ (4.5 Å), Trp 25 H^{N}−Trp 25 $H^{\epsilon 3}$ (4.0 Å), and Trp 25 $H^{\beta 3}$−Trp 25 $H^{\delta 1}$ (3.6 Å), were excluded from the final calculations since they proved to be incompatible with the majority of upper distance limits observed with the side chain of Trp 25 (see also below). No explicit hydrogen bond constraints were used.

The upper and lower distance constraints together with the dihedral angle constraints were used as input for structure calculations with the program DIANA. Starting from 100 random conformers, three REDAC cycles were used to improve the convergence of the DIANA algorithm. Thirty conformers with the lowest target functions were selected for further refinement. Restrained-energy refinement of these structures in the presence of a 6 Å water shell produced a set of conformers with low physical energies for the protein−protein interactions while only minimally affecting backbone and side chain conformation (Table 1). The 20 refined conformers with the lowest AMBER energies were selected

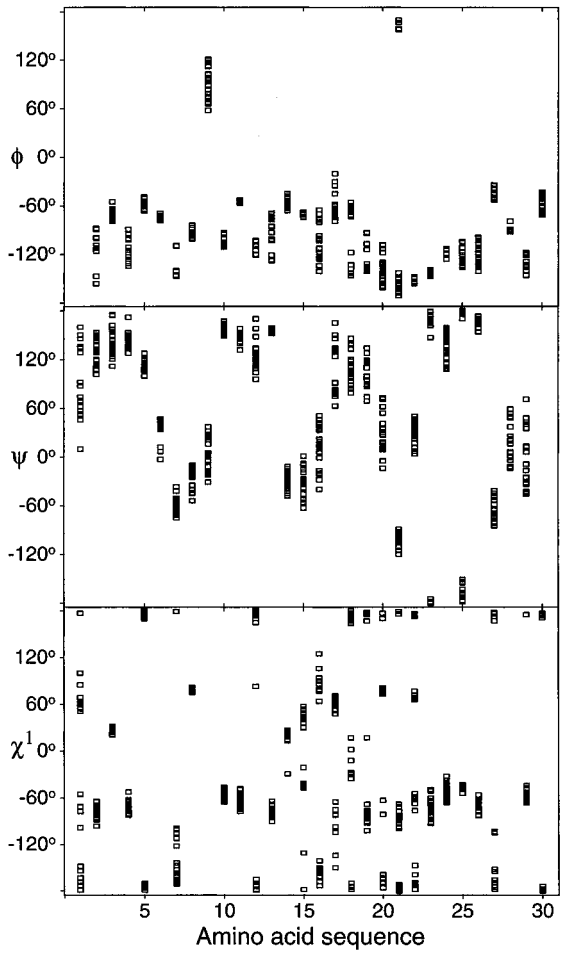

FIGURE 5: Plots of the dihedral angles ϕ, ψ, and χ^1 in the 20 conformers representing the NMR solution structure of the ZF-1−zinc complex *versus* the amino acid sequence.

to represent the NMR structure of the ZF-1−zinc complex. The mean energy of the protein−protein interactions in these 20 DIANA conformers decreased from −630 to −1081 kcal/mol as a result of the conjugate gradient minimization. The average pairwise rmsd to the mean conformer after energy minimization for residues 3−30 was 0.55 Å for the backbone atoms (N, C^α, and C′) and 1.12 Å for all heavy atoms excluding the zinc atom. Figure 5 displays the ϕ, ψ, and χ^1 angles versus the amino acid sequence of ZF-1. All pairs of ϕ and ψ angles are within or near the sterically allowed regions of the $\phi-\psi$ plane.

Solution Structure of the ZF-1−Zinc Complex. Figure 6A shows a stereoview of the 20 refined DIANA conformers displaying the backbone atoms (N, C^α, and C′) of all residues and the side chain heavy atoms of the zinc coordinating amino acids together with the zinc atom. The solution structure accounts for most of the observed amide proton exchange rates and allows the secondary structure elements to be defined with good accuracy. Table 2 lists the hydrogen bonds observed in more than half of the 20 conformers. No hydrogen bond is indicated for any of the very rapidly exchanging amide protons (Figure 4), and except for Tyr 13, all slowly exchanging amide protons are found to be hydrogen bonded (Table 2). The amide proton of Tyr 13 has an average solvent accessibility of less than 10% in the NMR structure which could account for its slow exchange. Hydrogen bonds are indicated in more than half of the NMR conformers for the amide protons of Cys 8, Cys 29, and Phe 30 for which neither very slow nor very fast amide proton exchange could be detected.

The secondary structure of the ZF-1−zinc complex consists of four short β-strands which are arranged into a loosely connected, strongly twisted antiparallel β-sheet (Figure 7). The irregularity of the sheet structure is also evidenced by the difficulties to delineate the β-strands by simple inspection of the data of Figure 4. Figure 8 presents an overview of the experimentally observed ROEs and slowly exchanging amide protons for residues involved in this secondary structure. The strands, numbered sequentially, comprise residues Pro 3 to Ala 6 (strand 1), Lys 10 to Val 12 (strand 2), Lys 17 to Asn 19 (strand 3), and Phe 24 to Lys 27 (strand 4). There are only two connectivities observed between strands one and four, namely, the hydrogen bond between Ala 6 H^N and Phe 24 O′ and the weak ROE between the α-protons of Cys 5 and Trp 25. The hydrogen bond between Trp 25 H^N and Val 18 O′ was found in only seven of the conformers, and the amide proton was not found experimentally to be slowly exchanging.

Between strands two and three there is a type III turn comprising residues 13−16 with the characteristic hydrogen bond between Gln 16 H^N and Tyr 13 O′ and the expected dihedral angles for Pro 14 and Thr 15 (Rose et al., 1985). At the C-terminus, the peptide fold ends with a type I turn comprising residues 26−29, where Cys 29 H^N makes a hydrogen bond with His 26 O′ and the residues Lys 27 and Ala 28 assume the ϕ and ψ angles characteristic of a type I turn (Rose et al., 1985).

Zinc Ion Coordination Site. The segment containing residues 5−10 forms a so-called "rubredoxin knuckle", a motif named after the iron-binding domains of rubredoxins (Adman et al., 1975) and present in numerous zinc-finger domains (Schwabe & Klug, 1994). The knuckle contains two of the four zinc-coordinating residues, namely, Cys 5 and Cys 8 with the characteristic bifurcated hydrogen bond between Cys 5 S^γ and the amide protons of Arg 7 and Cys 8 as well as the hydrogen bond between Cys 8 S^γ and Lys 10 H^N. The backbone hydrogen bonds Gly 9 H^N−Cys 5 O′ and Cys 5 H^N−Lys 10 O′ expected for a rubredoxin knuckle are also present in the solution structure of the ZF-1−zinc complex. The side chains of Cys 5 and Cys 8 are the side chains with the lowest solvent accessibility in the complex, and the zinc ion is well embedded in the interior of the structure with a calculated mean solvent accessibility of only 12%.

In the solution structure of the ZF-1−zinc complex, the nitrogen-bound $H^{\epsilon 2}$ proton of His 26 is hydrogen bonded to the backbone carbonyl of Ile 11 in a majority of the conformers, and in two conformers to a δ-oxygen of Glu 16. This explains why this histidine imidazole $H^{\epsilon 2}$ exchanges sufficiently slowly with solvent water to be observable in ^{1}H NMR spectra recorded using presaturation of the water resonance. It has been noted earlier that proteins coordinating zinc *via* histidine $N^{\delta 1}$ often form a hydrogen bond to the ϵ2 proton (Chakrabarti, 1990; Li & Tsai, 1993).

Comparison of the ZF-1−Zinc Complex with the CRP LIM2 Domain and CRIP. A LIM domain is commonly dissected into two distinct zinc-binding modules. Amino acid sequence comparison of the N- and C-terminal modules of CRP LIM2 and CRIP demonstrate that the homology is high within the modules (46% and 45% identity for both N- and C-terminal, respectively) but significantly lower between N- and C-terminal modules (∼21% identity). Extending the

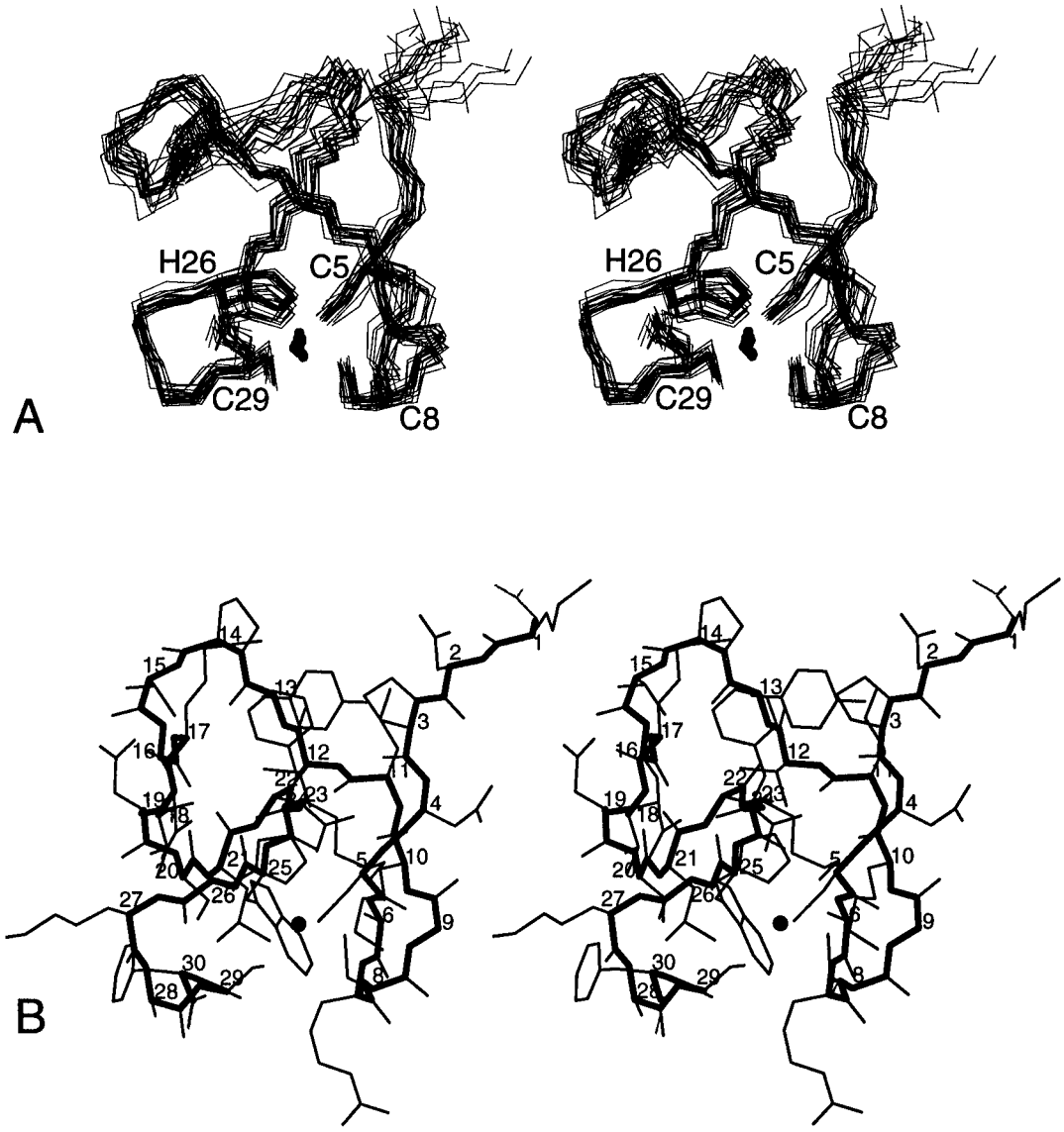

FIGURE 6: (A) Stereoview of the 20 refined DIANA structures. Structures are represented by lines connecting the backbone heavy atoms (N, C^{α}, and C′) following the superposition of these atoms for residues 3−30 for minimum rmsd with the mean conformer generated using this selection. In addition, the zinc atom and the side chains of the zinc-coordinating residues are shown. (B) Stereoview of the conformer with the smallest rmsd to the mean structure calculated from the 20 refined DIANA conformers. All heavy atoms are shown.

comparison to include ZF-1 allows its classification as an N-terminal module due to its greater homology to the N-terminal modules of CRP LIM2 and CRIP (50% and 43% identity, respectively) compared to the C-terminal modules (27% and 19% identity, respectively).

A superposition of the structure of the ZF-1−zinc complex with the corresponding residues (Figure 1) of the N-terminal zinc-binding modules of CRP LIM2 (Pérez-Alvarado et al., 1994) and CRIP (Pérez-Alvarado et al., 1996) shows the close similarity between the backbone conformations of the three modules (Figure 9). Superimposing the backbone atoms for the residues corresponding to residues 3−30 of ZF-1 gives an rmsd between the two mean structures of ZF-1 and CRP LIM2 of 1.57 Å, and for ZF-1 and CRIP an rmsd of 1.13 Å was calculated for this selection of backbone atoms. The differences between the amino terminal ends in all three structures may not be significant, since no NOE constraints were reported for Pro 1 in CRIP (Pro 3 in ZF-1) or the residues before Gly 117 in CRP LIM2 (Asn 4 in ZF-1).

We focus first on the comparison of ZF-1 with the N-terminal modules of CRP LIM2 and CRIP. The local rmsd between the structures of ZF-1 and CRP is smallest for the zinc-coordinating residues. A similarly small backbone rmsd is also found for the residues Glu 16, Lys 17, and Val 18 which are conserved in many LIM domains. Larger local rmsd values are, however, found for the likewise conserved residues Val 12 and Tyr 13. In fact, the largest differences between the backbone conformations of ZF-1 and CRP LIM2 are observed in the loop between Tyr 13 and Thr 15 of the ZF-1−zinc complex. This segment is less well-defined in the CRP LIM2 structure, since resonance assignments are missing for the residues corresponding to positions 14 and 15 in ZF-1. Yet, the differences appear to be real, since for some of the NOE constraints reported for CRP LIM2, no corresponding ROE cross-peak could be observed for the ZF-1−zinc complex. For example, the NOE Val 12 CH_3^{γ}−Glu 16 H^N was of sizable intensity in the CRP LIM2 protein but not observed in the ZF-1−zinc complex, although both residues are conserved between the two peptides. Scalar coupling constants cannot be compared for both peptides, since none were reported for CRP LIM2.

ZF-1 and CRIP are more similar in their backbone conformation than ZF-1 and CRP LIM2, as is clearly seen

Table 2: Hydrogen Bonds Found in the NMR Solution Structure of the ZF-1−Zinc Complex[a]

hydrogen donor		acceptor		number[b]
Hydrogen Bonds Between Backbone Amide Protons and Backbone Carbonyl Oxygens[c]				
Cys 5	H^N	Lys 10	O′	20
Ala 6	H^N	Phe 24	O′	11
Gly 9	H^N	Cys 5	O′	14
Val 12	H^N	Pro 3	O′	19
Glu 16	H^N	Tyr 13	O′	16
Val 18	H^N	Trp 25	O′	13
Cys 29	H^N	His 26	O′	20
Phe 30	H^N	His 26	O′	11
Hydrogen Bonds Involving Side Chain Atoms[c]				
His 26	$H^{\epsilon 2}$	Ile 11	O′	18
Hydrogen Bonds Involving Sulfur Atoms[d]				
Arg 7	H^N	Cys 5	S^γ	14
Cys 8	H^N	Cys 5	S^γ	15
Lys 10	H^N	Cys 8	S^γ	20

[a] The hydrogen bonds found in more than half of the 20 refined conformers using the following criteria for the donor−acceptor distance, d, and the angle between the donor−proton bond and the line connecting the donor and acceptor atoms, θ, are displayed. [b] The numbers in the last column indicate how many of the 20 energy refined conformers meet the criteria. [c] $d < 2.6$ Å and $\theta < 50°$. [d] $d < 2.8$ Å and $\theta < 50°$.

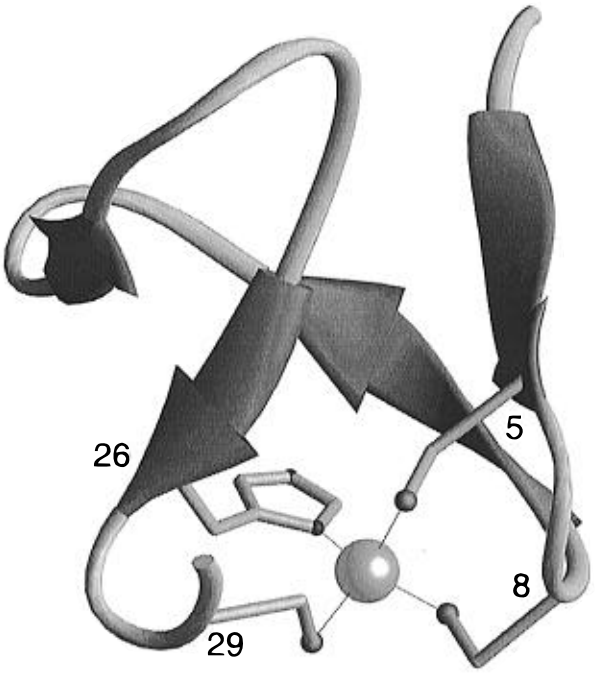

FIGURE 7: Ribbon representation of the ZF-1−zinc complex showing the four β strands drawn as arrows and the side chains of the zinc-coordinating residues in a ball-and-stick representation. Zinc is represented by a sphere, and the tetrahedral coordination is illustrated with solid lines. The drawing was generated with the program RIBBONS (Carson, 1991) using the refined DIANA conformer with the smallest rmsd to the mean structure.

in Figure 9. With the same superposition as above, the largest local rmsd values between their mean structures are for the N-terminal residues Pro 3 and Asn 4 (Pro 1 and Lys 2 in CRIP) and for the residues located after the third β-strand corresponding to Asn 19 to Lys 23 in ZF-1 (Arg 17 to Lys 21 in CRIP). Comparing ZF-1 and CRIP shows that the set of upper distance limit constraints of Asn 4 in ZF-1 is indistinguishable from the constraints observed with Lys 2 in CRIP, except for a weak NOE constraint Lys 2 H^α−His 24 $H^{\epsilon 1}$ (Asn 4 and His 26 in ZF-1) that was found for CRIP but not observed for ZF-1.

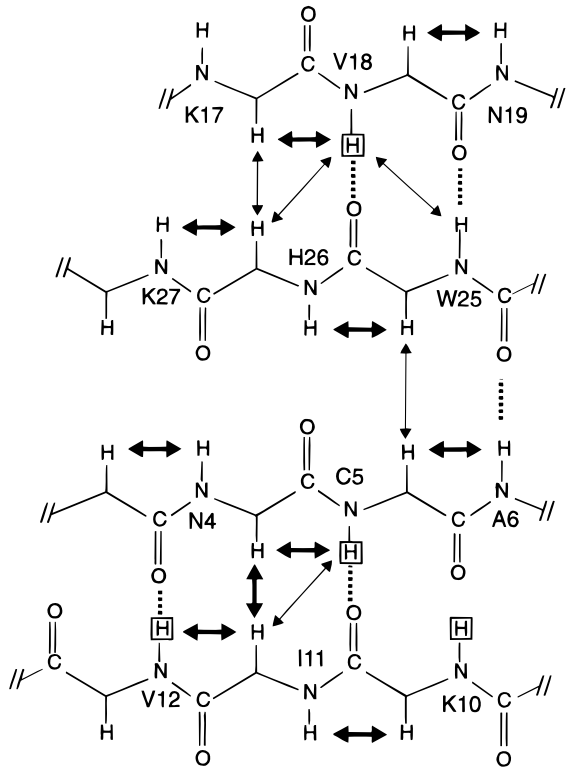

FIGURE 8: Diagram showing the measured ROEs/NOEs and hydrogen bonds identified in the refined DIANA structures defining the four β-strands in the ZF-1−zinc complex. Strong and weak NOEs are indicated with thick and thin arrows, respectively, and hydrogen bonds are illustrated with dotted lines. Boxes identify slowly exchanging amide protons (Figure 4). The hydrogen bond between the amide proton of Trp 25 and the carbonyl oxygen of Val 18 was observed in only seven of the 20 NMR conformers and is therefore not listed in Table 2.

Few significant differences in the experimental constraints were identified in the segment containing residues 19−23 of ZF-1 compared to CRIP which show the largest backbone rmsd values (1−2 Å, following global backbone superposition). For example, the NOE constraints for the backbone atoms in this region are very similar, but the $^3J_{H\alpha HN}$ coupling constants differ significantly for at least one residue: 8.3 Hz (Asp 22 in ZF-1, Figure 4) versus 4.8 and 5.6 Hz (Gly 20 in CRIP). A negative and a positive ϕ-angle resulted for this residue in the ZF-1−zinc complex and in CRIP, respectively. Most of the CRIP structure calculations used a set of hydrogen bond constraints which included constraints between Lys 21 H^N and Ser 18 O′ as well as between Ser 18 H^N and Lys 21 O′ (residues 23 and 20 in ZF-1). These two hydrogen bonds were observed in only four of the final conformers of the ZF-1−zinc complex, and only once did they both occur in the same conformer. Another significant difference in experimental constraints are the $^3J_{H\alpha HN}$ coupling constants in the segment comprising residues 7−11: Ile 11 in ZF-1 (Glu 9 in CRIP) shows a coupling constant of 2.8 Hz, but 7.2 Hz in CRIP, and Arg 7 in ZF-1 (Lys 5 in CRIP) shows a coupling constant of 9.7 Hz, but 7.4 Hz in CRIP. Yet, the backbone rmsd values for this segment are below 1.0 Å. Finally, different NOE constraints were observed for some of the conserved amino acid side chains. For example, a short upper distance limit constraint was reported between Val 16 H^N and Val 10 CH_3^γ in CRIP (residues 18 and 12 in ZF-1), but the corresponding cross-peak was absent in the NOESY and ROESY spectra of ZF-1.

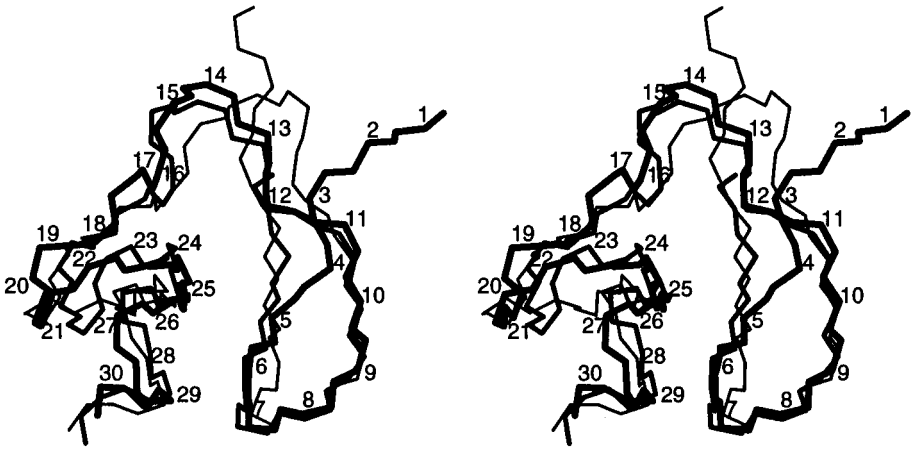

FIGURE 9: Stereoview showing a comparison of the ZF-1−zinc complex (thick line) with the first zinc-binding motif of the CRIP−zinc complex (medium-thick line) (Pérez-Alvarado et al., 1996) and the LIM2−zinc complex of CRP (thin line) (Pérez-Alvarado et al., 1994). The structures are drawn as lines connecting the backbone heavy atoms (N, C^{α}, and C′) following the superposition of these atoms for residues 116−143 of CRP, residues 1−28 of CRIP, and residues 3−30 of ZF-1 (Figure 1). The ZF-1 structure displayed is the refined DIANA conformer with the smallest rmsd to the mean structure calculated from the 20 refined DIANA conformers. The structures shown for CRIP and CRP LIM2 are those identified as representative by Pérez-Alvarado et al. (1994, 1996).

A hydrogen bond between His 139 $H^{\epsilon 2}$ and the side chain carboxyl group of Gly 129 was postulated for CRP LIM2 and the corresponding residues in CRIP (His 24 and Glu 14) based on the observation of strong NOEs between the histidine $H^{\delta 2}$ and the side chain protons of the glutamic acid (Pérez-Alvarado et al., 1994, 1996). We did observe the corresponding ROEs for the ZF-1−zinc complex, but the hydrogen bond with the glutamic acid is present in only two of the final conformers. This hydrogen bond is also absent in all of the NMR conformers of CRIP and CRP LIM2 using our criteria for hydrogen bond identification (Table 2). Instead, 18 of the 20 conformers of the ZF-1−zinc complex show a hydrogen bond between His 26 $H^{\epsilon 2}$ and the backbone carbonyl oxygen of residue 11 (Table 2). The corresponding hydrogen bond is also present in all NMR conformers of CRIP.

Overall, the structural variations between the N-terminal zinc-binding modules of the three LIM domains are small and most are within the precision of the structures. The rubredoxin knuckle motif is preserved as well as the Zn-coordinating residues. The similarity extends to the orientation of the hydrophobic side chains in the interior of the domains, like those of Val 12 and Trp 24 in ZF-1. The close similarity of the χ^1 and χ^2 angles of Trp 25 in ZF-1 and the corresponding Trp residues in CRP LIM2 and CRIP is remarkable, since the side chain of Trp 25 in ZF-1 showed at least four ROEs which could not be fulfilled by the present structure and had to be removed from the data input. The occurrence of these ROEs could be explained either by population of the rotamer around $\chi^1 = 60°$, or by changing the χ^2 angle by about 180°. However, the $\chi^1 = 60°$ rotamer should be populated only to a minor extent, since very different $^3J_{H\alpha H\beta}$ coupling constants were observed for the two β-protons. Similarly, a significant population of the alternative χ^2 rotamer would result in large violations of relatively strong ROEs. Interestingly, the ZF-1−zinc complex and the first zinc-binding modules of the CRP LIM2 domain and CRIP each coordinate zinc *via* histidine $N^{\delta 1}$, unlike the more usual coordination in other zinc-binding proteins *via* histidine $N^{\epsilon 2}$ (Schmiedeskamp & Klevit, 1994).

Extending the comparison with the ZF-1−zinc complex to include both N- and C-terminal modules of CRIP and CRP LIM2, we find that despite the limited sequence identiy between N- and C-terminal modules, including the change in zinc coordination from CCHC to CCCC, the backbone conformations are very homologous. For example, the backbone pairwise rmsd values between the mean structures of the ZF-1−zinc complex (residues 3−30) and the N- and C-terminal modules from CRIP (residues 1−28 and 28−55, respectively) are all less than 1.4 Å.

CONCLUSIONS

The ZF-1−zinc complex presented here is the third example of an N-terminal zinc-binding module of a LIM domain for which the three-dimensional structure has been determined. As expected from the large (>43%) sequence identity between the ZF-1−zinc complex and the N-terminal zinc-binding modules of CRP LIM2 and CRIP, the three structures are very similar. The similarities extend to the C-terminal modules and support the notion of a single conserved zinc-binding motif contained in LIM domains. In the N-terminal CCHC motif the zinc ion is coordinated by the imidazol N^{δ} and a so-called rubredoxin knuckle is formed by the segment containing the first two coordinating cysteines. The rubredoxin knuckle is also present in the C-terminal CCCC motifs as well as in numerous other zinc-finger motifs (Schwabe & Klug, 1994).

The present work demonstrates that the N-terminal zinc-binding module of a LIM domain is an independent folding unit. This result agrees well with the observation that the two zinc-binding modules of the LIM domains in CRP LIM2 and CRIP are differently orientated with respect to each other, corresponding to a rotation of about 60° (Pérez-Alvarado et al., 1996). The conformational restriction placed on the single zinc-finger motif present in LIM domains by zinc complexation coupled with the observed tolerance of amino acid substitution in certain segments of the polypeptide chain, makes it a particularly attractive building block for protein design and provides an explanation for both the abundance and variety of functions attributed to this fold in nature. In fact, nature already used zinc−ion complexation together with the rubredoxin knuckle motif as a building block in a number of other zinc-finger motifs.

ACKNOWLEDGMENT

We thank Prof. Jan Sjövall and Dr. William Griffiths for the mass spectroscopy measurements and Drs. Martin Billeter, Peter Güntert, and Lennart Nilsson for helpful discussions. In particular, we acknowledge the receipt of the coordinates and NMR constraints of CRP LIM2 and CRIP from Prof. Michael F. Summers and Dr. Gabriela Pérez-Alvarado prior to their public release.

SUPPORTING INFORMATION AVAILABLE

Table with the chemical shifts of the ZF-1−zinc complex and figure with the number of NOE constraints per residue used in the structure calculation and the local backbone and side chain rmsd values as a function of the amino acid sequence (2 pages). Ordering information is given on any current masthead page.

REFERENCES

Adman, E., Watenpaugh, E. D., & Jensen, L. H. (1975) *Proc. Natl. Acad. Sci. U.S.A. 72*, 4854−4858.

Arber, S., Halder, G., & Caroni, P. (1994) *Cell 79*, 221−231.

Atherton, E., & Sheppard, R. C. (1989) *Solid Phase Peptide Synthesis*, IRL Press, Oxford.

Aue, W. P., Bartholdi, E., & Ernst, R. R. (1976) *J. Chem. Phys. 64*, 2229−2246.

Bartels, C., Xia, T. H., Billeter, M., Güntert, P., & Wüthrich, K. (1995) *J. Biomol. NMR 6*, 1−10.

Bodenhausen, G., Kogler, H., & Ernst, R. R. (1984) *J. Magn. Reson. 58*, 370−388.

Braunschweiler, L., Bodenhausen, G., & Ernst, R. R. (1983) *Mol. Phys. 48*, 535.

Briand, J., & Ernst, R. R. (1991) *Chem. Phys. Lett. 185*, 276−285.

Carson, M. (1991) *J. Appl. Crystallogr. 24*, 958−961.

Chakrabarti, P. (1990) *Protein Eng. 4*, 57−63.

Cohen, B., McGuffin, E., Pfeifle, C., Segal, D., & Cohen, S. M. (1992) *Genes Dev. 6*, 715−729.

Cornell, W. D., Cieplak, P., Bayly, C. I., Gould, I. R., Merz, K. M., Ferguson, D. M., Spellmeyer, D. C., Fox, T., Caldwell, J. W., & Kollman, P. A. (1995) *J. Am. Chem. Soc. 117*, 5179−5197.

Crawford, A. W., Michelsen, J. W., & Beckerle, M. C. (1992) *J. Cell Biol. 116*, 1381−1393.

Crawford, A. W., Pino, J. D., & Beckerle, M. C. (1994) *J. Cell Biol. 124*, 117−127.

Ernst, R. R., Bodenhausen, G., & Wokaun, A. (1987) *Principles of Nuclear Magnetic Resonance in One and Two Dimensions*, Clarendon, Oxford.

Feuerstein, R., Wang, X., Song, D., Cooke, N. E., & Liebhaber, S. A. (1994) *Proc. Natl. Acad. Sci. U.S.A. 91*, 10655−10659.

Frankel, A. D., Berg, J. M., & Pabo, C. O. (1987) *Proc. Natl. Acad. Sci. U.S.A. 84*, 4841−4845.

Freyd, G., Kim, S. K., & Horvitz, R. (1990) *Nature 344*, 876−879.

Gill, N. G. (1995) *Structure 3*, 1285−1289.

Gross, E., & Meienhofer, J., Eds. (1981) *The Peptides: Analysis, Synthesis, Biology, Vol. 3, Protection of Functional Groups in Peptide Synthesis*, Academic Press, New York.

Güntert, P., & Wüthrich, K. (1991) *J. Biomol. NMR 1*, 447−456.

Güntert, P., Billeter, M., Braun, W., & Wüthrich, K. (1989) *J. Am. Chem. Soc. 111*, 3997−4004.

Güntert, P., Braun, W., & Wüthrich, K. (1991a) *J. Mol. Biol. 217*, 517−530.

Güntert, P., Qian, Y. Q., Otting, G., Müller, M., Gehring, W., & Wüthrich, K. (1991b) *J. Mol. Biol. 217*, 531−540.

Güntert, P., Dötsch, V., Wider, G., & Wüthrich, K. (1992) *J. Biol. NMR 2*, 619−629.

Kaptein, R. (1993) *Curr. Opin. Struct. Biol. 3*, 50−56.

Karlsson, O., Thor, S., Norberg, T., Ohlsson, H., & Edlund, T. (1990) *Nature 344*, 879−882.

Koradi, R., Billeter, M., & Wüthrich, K. (1996) *J. Mol. Graph. 14*, 51−55.

Klug, A., & Rhodes, D. (1987) *Trends Biochem. Sci. 12*, 464−469.

Kosa, J. L., Michelsen, J. W., Louis, H. A., Olsen, J. I., Davis, D. R., Beckerle, M. C., & Winge, D. R. (1994) *Biochemistry 33*, 468−477.

Hempe, J. M., & Cousins, R. J. (1991) *Proc. Natl. Acad. Sci. U.S.A. 88*, 9671−9674.

Li, Y., & Tsai, M. (1993) *J. Am. Chem. Soc. 115*, 8523−8526.

Liepinsh, E., Berndt, K. D., Sillard, R., Mutt, V., & Otting, G. (1994) *J. Mol. Biol. 239*, 137−153.

Luisi, B. F., Xu, W. X., Otwinowski, Z., Freedman, L. P., Yamamoto, K. R., & Sigler, P. B. (1991) *Nature 352*, 497−505.

Michelsen, J. W., Schmeichel, K. L., Beckerle, M. C., & Winge, D. R. (1993) *Proc. Natl. Acad. Sci. U.S.A. 90*, 4404−4408.

Mizuno, K., Okano, I., Ohashi, K., Nunoue, K., Kuma, K., Miyata, T., & Nakamura, T. (1994) *Oncogene 9*, 1605−1612.

O'Dell, B. L. (1992) *Nutrition Rev. 50*, 232−233.

Omichinski, J. G., Clore, G. M., Schaad, O., Felsenfeld, G., Trainor, C., Appella, E., Stahl, S. J., & Gronenborn, A. M. (1993) *Science 261*, 438−446.

Otting, G., Liepinsh, E., Farmer, B. T., II, & Wüthrich, K. (1991) *J. Biomol. NMR 1*, 209−215.

Párraga, G., Horvath, S. J., Eisen, A., Taylor, W. E., Hood, L., Young, E. T., & Klevit, R. E. (1988) *Science 241*, 1489−1492.

Pérez-Alvarado, G. C., Miles, C., Michelsen, J. W., Louis, H. A., Winge, D. R., Beckerle, M. C., & Summers, M. F. (1994) *Nature Struct. Biol. 1*, 388−398.

Pérez-Alvarado, G. C., Kosa, J. L., Louis, H. A., Beckerle, M. C., Winge, D. R., & Summers, M. F. (1996) *J. Mol. Biol. 257*, 153−174.

Rance, M., Sørensen, O. W., Bodenhausen, G., Wagner, G., Ernst, R. R., & Wüthrich, K. (1983) *Biophys. Res. Commun. 117*, 479−485.

Richmond, T. J. (1984) *J. Mol. Biol. 178*, 63−89.

Rose, G. D., Gierasch, L. M., & Smith, J. A. (1985) *Protein Chem. 37*, 1−109.

Sanchez-Garcia, I., & Rabbitts, T. H. (1994) *Trends Genet. 10*, 315−320.

Schmeichel, K. L., & Beckerle, M. C. (1994) *Cell 79*, 211−219.

Schwabe, J. W. R., & Klug, A. (1994) *Nat. Struct. Biol. 1*, 345−349.

Schmiedeskamp, M., & Klevit, R. E. (1994) *Curr. Opin. Struct. Biol. 4*, 28−35.

Sillard, R., Jörnvall, H., Carlquist, M., & Mutt, V. (1993) *Eur. J. Biochem. 211*, 377−380.

South, T. L., Blake, P. R., Hare, D. R., & Summers, M. F. (1991) *Biochemistry 30*, 6342−6349.

Summers, M. F., South, T. L., Kim, B., & Hare, D. R. (1990) *Biochemistry 29*, 329−340.

Szyperski, T., Güntert, P., Otting, G., & Wüthrich, K. (1992) *J. Magn. Reson. 99*, 552−560.

Taira, M., Evrard, J. L., Steinmetz, A., & Dawid, I. B. (1995) *Trends Genet. 11*, 431−432.

Tomasetto, C., Régnier, C., Moog-Lutz, C., Mattei, M. G., Chenard, M. P., Lidereau, R., Basset, P., & Rio, M. C. (1995a) *Genomics 28*, 367−376.

Tomasetto, C., Moog-Lutz, C., Régnier, C. H., Schreiber, V., Basset, P., & Rio, M. C. (1995b) *FEBS Lett. 373*, 245−249.

Way, J. C., & Chalfie, M. (1988) *Cell 54*, 5−16.

Weiskirchen, R., Pino, J. D., Macalma, T., Bister, K., & Beckerle, M. C. (1995) *J. Biol. Chem. 270*, 28946−28954.

Wüthrich, K. (1986) *NMR of Proteins and Nucleic Acids*, Wiley, New York.

Xia, T. H. (1992) Ph.D. Thesis No. 9831, ETH Zürich, Switzerland.

BI961149J